MF-LRTC: MULTI-FILTERS GUIDED LOW-RANK TENSOR CODING FOR IMAGE RESTORATION

Hongyang Lu, Sanqian Li, Qiegen Liu, Yuhao Wang*
Department of Electronic Information Engineering, Nanchang University, Nanchang, 330031, China

ABSTRACT

Image prior information is a determinative factor to tackle with the ill-posed problem. In this paper, we present a multi-filters guided low-rank tensor coding (MF-LRTC) model for image restoration. The appeal of constructing a low-rank tensor is obvious in many cases for data that naturally comes from different scales and directions. The MF-LRTC takes advantages of the low-rank tensor coding to capture the sparse convolutional features generated by multi-filters representation. Using such a low-rank tensor coding would reduce the redundancy between feature vectors at neighboring locations and improve the efficiency of the overall sparse representation. In this work, we are committed to achieving this goal by convoluting the target image with filters to formulate multi-features images. Then similarity-grouped cube set extracted from the multi-features images is regarded as a low-rank tensor. The potential effectiveness of this tensor construction strategy is demonstrated in image restoration including image deblurring and compressed sensing (CS) applications.

Index Terms—Image restoration, Multi-filters, Low-rank tensor coding, HOSVD decomposition.

1. INTRODUCTION

Multi-view representations of images have become a standard tool in image analysis. Such representations offer a number of advantages over one-view or image domain based methods. Since they represent distinct but complementary information that exists at various scales, they have great potential for improving performance in compressive sensing (CS), image super-resolution and deblurring, etc.[1, 2, 3].

Due to the successful modeling of images by nonlocal and self-similarity properties, image patch-based approaches have attracted lots of attentions in past few years [4, 5, 6, 7, 8]. Unfortunately, it is well known that partial representation of patches only allows finding neighbors in a specific type of feature space, and image patches do not strictly follow the similar structure at different scale/resolution spaces. As stated in ref. [2], in many real-world scenarios, each object can be described by multiple sets of features, where each feature describes a view of the same set of underlying objects. Specifically, for a patch in image processing community, each feature that summarizing the image patch can be considered as a view of the patch. How to find multi-view representation that describes the patch character heterogeneously and integrates them into a unified representation for subsequent processing is a promising research direction. Therefore, a redundancy and complemental multi-view representation of patches will be more beneficial to reveal the underlying visual manifold.

Low-rank matrix approximation has been successfully applied to numerous vision problems in recent years. Several existing works have indicated that there are many repetitive image structures in an image. As pointed out by refs. [4, 9], an advanced sparse representation method which considers local spatial property, can be approximated by low-rank approach. However, two-dimensional low-rank model cannot fully exploit the correlation in multidimensional data sets such as multispectral data. As a more general tool, low-rank tensor has gained more and more attentions to describe the high-dimensional data [10, 11, 12, 13, 14, 15, 16, 17]. Building on recent studies about matrix completion using the matrix trace norm, Liu *et al.* [10] developed three low-rank tensor completion (LRTC) algorithms to solve the tensor completion of convex optimization.

Instead of the above local approaches that viewed the whole data as a low-rank tensor, some researchers considered some clustered elements in the whole data as a low-rank tensor, via the nonlocal strategy. For denoising purpose, Rajwade *et al.* [18] proposed to group together similar patches from a noisy image into a 3D stack and manipulate the higher-order singular value decomposition (HOSVD) coefficients of this stack by hard thresholding to produce the final filtered image.

The investigation of multi-view features to facilitate image restoration has appealed to many researchers. Generally, the complementary information of distinct characteristics is exploited to reveal different physical meanings and statistical properties of patches, hence a better manifold structure is utilized. In this paper, we further go ahead to exploit the high-dimensional property of the multi-features by low-rank tensor formulation, and apply it to image deblurring and CS recovery. Fig. 1 shows the exploration of the proposed algorithm. The proposed algorithm exploits the local correlation

This work was supported in part by the National NSFC under 61503176, 61362001, 6166103.
*Correspondence author. E-mail: liuqiegen@ncu.edu.cn.

presented among voxels in each cube and the nonlocal correlation between the corresponding voxels of different cubes.

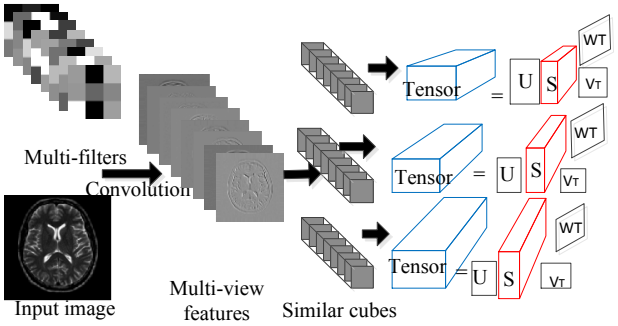

Fig. 1. Exploration of multi-filters guided low-rank tensor coding for image restoration.

2. MF-LRTC: MULTI-FILTERS GUIDED LOW-RANK TENSOR CODING

In this work, the rationales of the used convolutional-derived feature images and the low-rank tensor formulation are discussed, and then the present method MF-LRTC is derived.

2.1. Multi-filters Induced Feature

Many of works utilized the first-order gradient filters with different orientations and two-order LapLacian filters [19, 20]. For natural image oriented high-order Markov random field such as Filed-of-Experts (FoE) [21, 22], the neighborhood constraint is defined as

$$p = (x;\Theta) = (1/Z(\Theta)) \prod_{n=1}^{N} \prod_{k=1}^{K} \phi(J_k^T x_n; \alpha_k) \tag{1}$$

where $J_k^T x_n$ denotes the convolution of image x_n with FoE filter J_k, $\phi(\bullet)$ is an expert function, α_k is the parameter of the k-th filter, K is the number of total filters, and $Z(\Theta)$ is the partition function for normalization. These higher-order and multi-frequency models are able to capture the structures in natural images that cannot be captured by only using the first derivatives as in first-order gradient filters. Thus, the trained FoE filters have more powerful characterization ability. FoE filters have extensive applications in image processing such as image inpainting, denoising and deblurring. Interested readers please refer to refs. [23, 24].

In this paper, we mean to exploit certain convolutional characteristics and obtain multi-view features to form low-rank tensor. The convolutional characteristics are defined as:

$$u_1 = J_1^T u;\ \cdots;\ u_k = J_k^T u;\ \cdots;\ u_K = J_K^T u; \tag{2}$$

where $\{J_k, k = 1, \cdots, K\}$ are elaborately designed kernel functions which extracted image features out of image u; $J_k^T u$ denotes the convolution of image u with FoE filter J_k. The associate multi-view features exhibit two characteristics: sparsity and redundancy. Fig. 2(a) illustrates one learned FoE filter set. Fig. 2(b) shows the corresponding guided multi-view features by applying the multi-filters in Fig. 2(a). As can be expected, each filtered patch can be properly characterized by multiple visual features, and multi-view are presented and complementary to each other.

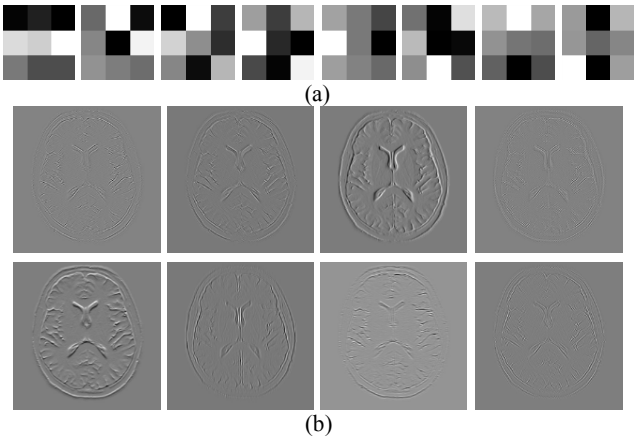

Fig. 2. Visualization of multi-filters and guided multi-features. (a) Different multi-filters. (b) The corresponding multi-view features guided according to (a).

2.2. Low-rank Tensor Approximation

Similar to refs. [25, 26], prior to the low-rank tensor approximation, it needs to use non-local strategy to form high-dimensional tensor by cubes grouping. First, we extract 3D cubes from multi-view features of size $H \times W \times K$; for each exemplar cube $\mathcal{P}_i$, we search for m similar cubes within a local neighbor region via k-nearest neighbor method. Second, we group the m 3D cubes into a 3-order tensor by reshaping each local window matrix slice of 3D cubes into 1D vectors and stack the similar cubes accordingly. As a consequence, the 3-order tensor $\mathcal{Y}_i \in \mathbb{R}^{n \times m \times K}$ is defined.

Generally, the HOSVD of the tensor $\mathcal{X}_i$ is given as follow:

$$\begin{aligned} \mathcal{X}_i &= \sum_{r=1}^{n} \sum_{c=1}^{m} \sum_{k=1}^{K} \tilde{\mathcal{S}}_i(r,c,k) u_{i,r} \times v_{i,c} \times w_{i,k} \\ &= \tilde{\mathcal{S}}_i \times_1 \mathrm{U}_i \times_2 \mathrm{V}_i \times_3 \mathrm{W}_i \end{aligned} \tag{3}$$

where $\mathrm{U}_i = [u_{i,1}, \ldots, u_{i,n}] \in \mathbb{R}^{n \times n}$, $\mathrm{V}_i = [v_{i,1}, \ldots, v_{i,m}] \in \mathbb{R}^{m \times m}$ and $\mathrm{W}_i = [w_{i,1}, \ldots, w_{i,K}] \in \mathbb{R}^{K \times K}$ are orthogonal matrices, $\tilde{\mathcal{S}}_i \in \mathbb{R}^{n \times m \times K}$ is the 3D coefficient array which called core tensor, $\tilde{\mathcal{S}}_i(r,c,k)$ is the component of $\tilde{\mathcal{S}}_i$, $\times$ denotes the tensor product, and $\times_j$ denotes the j-th model tensor product. Three orthogonal matrices U_i, V_i, and W_i can be computed from SVD of model-j ($j = 1,2,3$) flattening of $\mathcal{X}_i$ respectively. Thanks for the grouping of similar cubes, a low-rank tensor $\mathcal{Y}_i$ can be approximated as follow:

$$\begin{aligned} \hat{\mathcal{Y}}_i &= \sum_{r=1}^{r_1} \sum_{c=1}^{r_2} \sum_{k=1}^{r_3} \hat{\mathcal{S}}_i(r,c,l) u_{i,r} \times v_{i,c} \times w_{i,k} \\ &= \hat{\mathcal{S}}_i \times_1 \hat{\mathrm{U}}_i \times_2 \hat{\mathrm{V}}_i \times_3 \hat{\mathrm{W}}_i \end{aligned} \tag{4}$$

where $\hat{\mathrm{U}}_i = [u_{i,1}, \ldots, u_{i,r_1}] \in \mathbb{R}^{n \times r_1}$, $\hat{\mathrm{V}}_i = [v_{i,1}, \ldots, v_{i,r_2}] \in \mathbb{R}^{m \times r_2}$ and $\hat{\mathrm{W}}_i = [w_{i,1}, \ldots, w_{i,r_3}] \in \mathbb{R}^{K \times r_3}$ are the thin matrices associated with U_i, V_i, and W_i respectively. $r_1 \le n$, $r_2 \le m$, and $r_3 \le K$, and $\hat{\mathrm{S}}_i \in \mathbb{R}^{r_1 \times r_2 \times r_3}$ denotes the smaller core tensor. With the estimated

rank parameters (r_1, r_2, r_3), low-rank tensor approximation can be obtained by setting the last $n-r_1$, $m-r_2$, and $K-r_3$ values along each mode in $\tilde{s}_i$ to be zero values. Alternatively, this procedure can be approximated by enforcing the core tensor $\tilde{s}_i$ to be sparse [18, 27, 28].

2.3. Proposed MF-LRTC

Generally, in the scenario of image recovery problem, the observed data is modeled as $y = Au + n$, where A is a general measurement operator and n is the additive Gaussian noise. The recovery of u from y can be achieved by solving the following minimization problem:

$$\{u, \mathcal{Y}\} = \arg\min_{u,\mathcal{Y}} \sum_{i=1}^{N} \left\{ \frac{1}{2} \left\| \tilde{\mathbf{R}}_i [J_1^T u, \cdots, J_K^T u] - \mathcal{Y}_i \right\|_2^2 + \tau rank(\mathcal{Y}_i) \right\} + \frac{\nu_2}{2} \left\| y\text{-}Au \right\|_2^2 \quad (5)$$

where $J_k^T u$ denotes the convolution of image u with FoE filter J_k, ν_2 balances the regularization term and data-fidelity term, τ is the weighting parameter for the low-rank coding term. $\tilde{\mathbf{R}}_i = \left[\tilde{\mathbf{R}}_{i0}, \tilde{\mathbf{R}}_{i1}, \cdots, \tilde{\mathbf{R}}_{im-1} \right]$ denotes the operator for extracting similar cubes. We extract exemplar cubes $\tilde{\mathbf{R}}_i [J_1^T u, \cdots, J_K^T u]$ at every i voxels along each direction and group a set of similar cubes.

We use the augmented Lagrangian and ADMM to solve Eq.(5). The Eq. (5) can be rewritten as follows by introducing auxiliary variable $b = \{b_1, \cdots, b_K\}$.

$$\{u, \mathcal{Y}, b\} = \arg\min_{u,\mathcal{Y},b} \sum_{i=1}^{N} \left\{ \frac{1}{2} \left\| \tilde{\mathbf{R}}_i b - \mathcal{Y}_i \right\|_2^2 + \tau rank(\mathcal{Y}_i) \right\} + \frac{\nu_2}{2} \left\| Au - y \right\|_2^2 \quad (6)$$
$$s.t. \quad b_k = J_k^T u, \quad k = 1, 2, \cdots, K$$

Then, by introducing the augmented Lagrangian algorithm, we obtain a sequence of constrained sub-problems as follows:

$$\{u^{j+1}, \mathcal{Y}^{j+1}, b^{j+1}\} = \arg\min_{u,\mathcal{Y},b} \sum_{i=1}^{N} \left\{ \frac{1}{2} \left\| \tilde{\mathbf{R}}_i b - \mathcal{Y}_i \right\|_2^2 + \tau rank(\mathcal{Y}_i) \right\} + \frac{\nu_2}{2} \left\| Au - y \right\|_2^2 + \frac{\mu}{2} \sum_{k=1}^{K} \left\| \lambda_k^j + J_k^T u - b_k \right\|_2^2 \quad (7)$$

$$\lambda_k^{j+1} = \lambda_k^j + J_k^T u^{j+1} - b_k^{j+1} \quad (8)$$

where μ denotes the augmented Lagrangian parameter. Empirically, it has little impact on the final reconstruction quality provided it is sufficiently small. The superscript j denotes the iteration number.

The ADMM can be used to address the minimization of Eq. (7) with respect to u, $\mathcal{Y}$, and b. This technique carries out approximation via alternating minimization with respect to one variable while keeping other variables fixed.

The overall procedure of entire MF-LRTC algorithm can be summarized below as **Algorithm 1**. In **Algorithm 1**, it consists of shrinkage operations that are fast to calculate as they correspond to pixel-wise operations, and a Fourier-based reconstruction that can be performed efficiently. The multi-view features cube-matching operation in our case is similar as the traditional patch-matching implementation, and we perform a variant of k-nearest-neighbor search with a local window.

Algorithm 1: MF-LRTC

Initialization:

(1) Estimate an initial image u^0 using a standard recovery method (e.g., DCT/zero-filled based recovery method);

(2) Set parameters μ, τ, ν_2, K, J;

(3) Obtaining the multi-view features $J_k^T u^0$;

(4) **For** $j = 1, 2, \cdots, J$

(a) Grouping a set of cubes $\tilde{\mathbf{R}}_i(b^{j+1}), i = 1, \cdots, N$;

(b) Low-rank tensor approximation $\mathcal{Y}_i$;

(c) Update $u^{j+1}, b^{j+1}, \lambda^{j+1}$;

(5) **End (For)**

3. APPLICATIONS

The performances of the proposed method MF-LRTC is evaluated and compared with different state-of-the-art algorithms. Diverse images including natural images and medical images are tested. In all the experiments, unless otherwise stated, we use a fixed FoE filter set, denoted by csf_3×3 kernel, to construct 8 different multi-view features. Both quantitative and qualitative experiments validate the effectiveness of proposed algorithms. We use the peak signal-to noise ratio (PSNR) to evaluate the quality of restoration.

3.1. Image Deblurring

The image deblurring application is conducted by Gaussian blurring kernel with $\sigma = 3$ under different additive Gaussian white noise. The Gaussian white noises with standard deviation $\text{std} = \sqrt{2}$, and $\text{std} = 2$ are added. The proposed method is compared with the constrained TV deblurring method TV, L0-Abs [1], Bayesian-TV [29], and ASDS-TD2 [6]. The PSNR results obtained by the competing methods are listed in Table 1. One can be seen that the latter two adaptively patch-based methods outperform the former three local methods, via exploiting the nonlocal redundancies in the image. Particularly, the PSNR values of improvement of MF-LRTC over the ASDS-TD2 method are 1.93 dB at $\text{std} = \sqrt{2}$ and 1.06 dB at $\text{std} = 2$ for the tested image Cameraman, respectively.

Table 1.PSNR results of five methods (TV, L0-Abs, Bayesian-TV, ASDS-TD2, MF-LRTC) at Gaussian blur kernel with different noise levels (top line: $\text{std} = \sqrt{2}$, bottom line: $\text{std} = 2$)

Test image	TV	L0-Abs	Bayesi-an-TV	ASDS-TD2	MF-LRTC
Camer-aman	23.08	23.51	22.59	23.90	**25.83**
	22.93	23.25	22.36	23.76	**24.82**
Peppers	25.96	26.61	24.94	26.79	**27.69**
	25.72	26.24	24.38	26.06	**26.97**

3.2. CS Recovery

In this subsection, we conduct the CS recovery experiment to evaluate the performance of proposed method. Two sampling

schemes, the 2D random under-sampling and pseudo radial under-sampling with ratios (63%, 73%, and 80%), are conducted to generate the partial Fourier measurements, respectively.

The present MF-LRTC method is compared with DLMRI [30], Grad-DL[5], NLR-CS-baseline [4]. Both DLMRI and Grad-DL method utilize the popular K-SVD dictionary learning to represent the underlying data. The parameters of DLMRI are set as the default values. The Grad-DL method followed the same setup, with additional choices of $\lambda_1 = 60$ and $\nu_2 = 3$ based the reference experimental results. NLR-CS-baseline utilized the convex l_1-based nuclear norm to approximate the rank penalty. The main parameters of MF-LRTC for each exemplar are set as follows: patch size is set to be 4×4 and total $m = 25$ similar cubes are selected for each exemplar cubes, μ =0.005, τ =0.1, and ν_2 is tuned separately for each under-sampling rate.

The reconstruction performance with different under-sampling schemes and ratios are evaluated. Table 2 shows the corresponding PSNR comparison results of four methods with different images. First, for the whole table, it can be observed that the latter two nonlocal low-rank methods achieve much higher PSNR values than the former two dictionary learning methods. The reasons may come from many aspects. It should be noted that both DLMRI and Grad-DL are initialized with the zero-filled Fourier reconstruction result. On the other hand, both the two low-rank approaches use the DCT based recovery method output as initialization estimation.

To facilitate the evaluation of subjective qualities, we compare the reconstructed MR images by four state-of-the-art methods for variable density 2D random under-sampling in Fig. 3. The under-sampling rates is 80%. It can be seen that MF-LRTC method recovers the underlying information more effectively, in terms of large-scale sharp edges and fine-scale image details. Fig. 4 shows the results for the pseudo radial under-sampling scheme with 63% rates. Although all methods present excellent performances on suppressing aliasing artifacts, our MF-LRTC provides a better reconstruction of object edges and preserved finer texture information. The associated errors of methods NLR-CS-baseline [4] and MF-LRTC are depicted in the last two columns, respectively.

Table 2. The reconstruction PSNR values of four methods at under-sampling percentages with 63%, 73%, and 80%.

	Test image	under-sampling ratio	DLMRI	Grad-DL	NLR-CS-base	MF-LRTC
2D Random	T2axialbrain	63%	38.52	43.75	48.72	**48.81**
		73%	36.77	40.84	45.22	**45.43**
		80%	35.22	38.42	42.26	**42.95**
	Herni-ateddis-dis-clspine	63%	39.45	42.21	46.53	**47.60**
		73%	37.40	39.67	43.28	**44.60**
		80%	35.64	37.33	39.31	**41.47**
Pseudo Radial	T2axialbrain	63%	36.68	39.54	42.96	**44.01**
		73%	34.87	36.65	39.24	**39.55**
		80%	32.75	33.88	36.31	**36.73**
	Herni-ateddis-dis-clspine	63%	36.77	37.08	42.83	**43.55**
		73%	34.92	34.85	38.90	**39.12**
		80%	33.03	32.30	35.44	**35.99**

4. CONCLUSIONS

In this paper, a novel multi-view features guided low-rank tensor coding is presented for the image restoration. The proposed MF-LRTC efficiently characterizes the intrinsic structured sparsities of natural images by exploiting both locally multi-scale property and nonlocal multi-dimensional sparsity simultaneously. The benefits of the multi-filters are demonstrated for applications. We believe that this mechanism has potential for many other image processing tasks such as super resolution, replacing both the standard low-rank tensor and the features used in these applications.

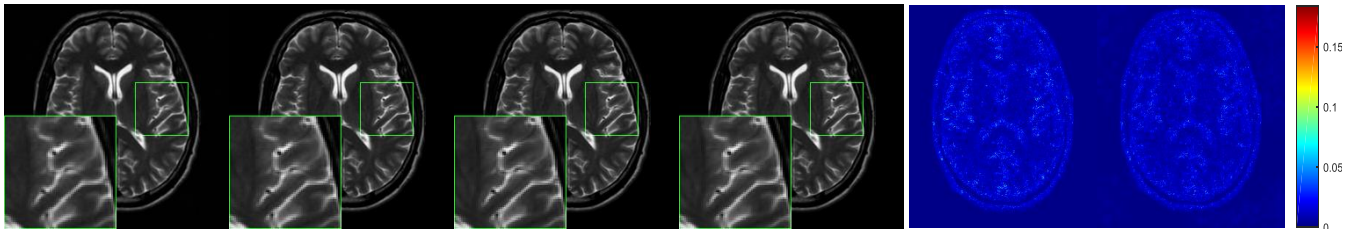

Fig. 3. CS recovered results with 2D random under-sampling scheme by DLMRI [30], Grad-DL [5], NLR-CS-baseline [4], and MF-LRTC. The last two columns are the associated errors of NLR-CS-baseline [4] and MF-LRTC.

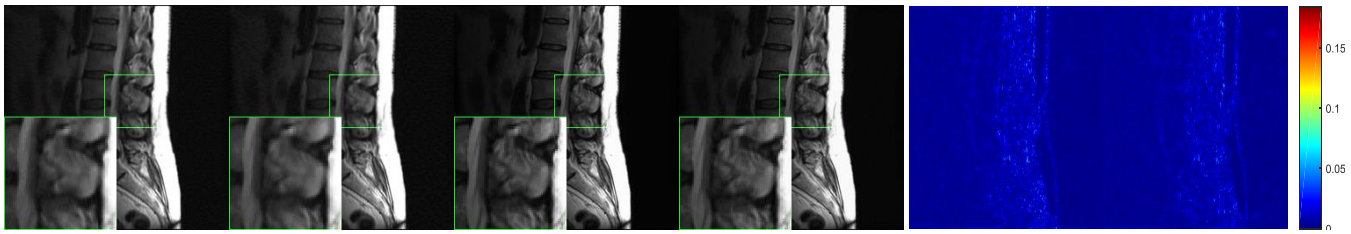

Fig. 4. CS recovered MR images with pseudo radial under-sampling scheme by DLMRI [30], Grad-DL [5], NLR-CS-baseline [4], and MF-LRTC. The last two columns are the associated errors of NLR-CS-baseline [4] and MF-LRTC.

5. REFERENCES

[1] J. Portilla, "Image restoration through l0 analysis-based sparseoptimization in tight frames," *in (ICIP)*, pp. 3909-3912. 2009.

[2] T. Xia, D. Tao, T. Mei, and Y. Zhang, "Multiview spectral embedding," *IEEE Transactions on Systems, Man, and Cybernetics, Part B (Cybernetics)*, vol. 40, no. 6, pp. 1438-1446, 2010.

[3] C. Hong, Y. Dit-Yan, and X. Yimin, "Super-resolution through neighbor embedding," *in (CVPR). Proceedings of the 2004 IEEE Computer Society Conference on*, pp. I-I. 2004.

[4] W. Dong, G. Shi, X. Li, Y. Ma, and F. Huang, "Compressive sensing via nonlocal low-rank regularization," *IEEE Trans. Image Process,* vol. 23, no. 8, pp. 3618-3632, 2014.

[5] Q. Liu, S. Wang, L. Ying, X. Peng, Y. Zhu, and D. Liang, "Adaptive dictionary learning in sparse gradient domain for image recovery," *IEEE Trans. Image Process*, vol. 22, no. 12, pp. 4652-4663, 2013.

[6] W. Dong, L. Zhang, G. Shi, and X. Wu, "Image deblurring and super-resolution by adaptive sparse domain selection and adaptive regularization," *IEEE Trans. Image Process*, vol. 20, no. 7, pp. 1838-1857, 2011.

[7] Q. Liu, S. Wang, K. Yang, J. Luo, Y. Zhu, D. Liang, "Highly undersampled magnetic resonance image reconstruction using two-level Bregman method with dictionary updating," *IEEE Trans. Med. Imag.*, vol. 32, no. 7, pp. 1290-1301, Jul. 2013.

[8] H. Lu, J. Wei, L. Wang, P. Liu, Q. Liu, Y. Wang, X. Deng, "Reference information based remote sensing image reconstruction with generalized nonconvex low-rank approximation," *Remote Sensing*, vol. 8, no. 6, 2016.

[9] W. Dong, G. Shi, and X. Li, "Nonlocal image restoration with bilateral variance estimation: a low-rank approach," *IEEE Trans. Image Process*, vol. 22, no. 2, pp. 700-711, 2013.

[10] J. Liu, P. Musialski, P. Wonka, and J. Ye, "Tensor completion for estimating missing values in visual data," *IEEE Trans. Pattern Analysis and Machine Intelligence*, vol. 35, no. 1, pp. 208-220, 2013.

[11] D. Kressner, M. Steinlechner, and B. Vandereycken, "Low-rank tensor completion by Riemannian optimization," *BIT Numerical Mathematics*, vol. 54, no. 2, pp. 447-468, 2013.

[12] Y. L. Chen, C. T. Hsu, and H. Y. M. Liao, "Simultaneous tensor decomposition and completion using factor priors," *IEEE Trans. Pattern Analysis and Machine Intelligence*, vol. 36, no. 3, pp. 577-591, 2014.

[13] A. Narita, K. Hayashi, R. Tomioka, and H. Kashima, "Tensor factorization using auxiliary information," *Data Mining and Knowledge Discovery*, vol. 25, no. 2, pp. 298-324, 2012.

[14] T.-Y. Ji, T.-Z. Huang, X.-L. Zhao, T.-H. Ma, and G. Liu, "Tensor completion using total variation and low-rank matrix factorization," *Information Sciences*, vol. 326, pp. 243-257, 2016.

[15] J. He, Q. Liu, A. Christodoulou, C. Ma, F. Lam, and Z. P. Liang, "Accelerated high-dimensional MR imaging with sparse sampling ssing sow-sank sensors," *IEEE Trans Med Imaging*, Apr 12, 2016.

[16] G. Bergqvist, and E. G. Larsson, "The higher-order singular value decomposition: theory and an application," *IEEE Signal Processing Magazine*, vol. 27, no. 3, pp. 151-154, 2010.

[17] L. Grasedyck, D. Kressner, and C. Tobler, "A literature survey of low-rank tensor approximation techniques," *GAMM-Mitteilungen*, vol. 36, no. 1, pp. 53-78, 2013.

[18] A. Rajwade, A. Rangarajan, and A. Banerjee, "Image denoising using the higher order singular value decomposition," *IEEE Trans. Pattern Analysis and Machine Intelligence,* vol. 35, no. 4, pp. 849-862, 2013.

[19] X. Peng, and D. Liang, "MR image reconstruction with convolutional characteristic constraint (CoCCo)," *IEEE Signal Processing Letters*, vol. 22, no. 8, pp. 1184-1188, 2015.

[20] S. Yang, Z. Wang, L. Zhang, and M. Wang, "Dual-geometric neighbor embedding for image super resolution with sparse tensor," *IEEE Trans. Image Process*, vol. 23, no. 7, pp. 2793-2803, 2014.

[21] S. Roth, and M. J. Black, "Fields of Experts," *International Journal of Computer Vision*, vol. 82, no. 2, pp. 205-229, 2009.

[22] U. Schmidt and S. Roth, "Shrinkage fields for effective image restoration," in *(CVPR), IEEE Conference on*, pp. 2774-2781. 2014.

[23] U. Schmidt, C. Rother, S. Nowozin, J. Jancsary, and S. Roth, "Discriminative non-blind deblurring."in *(CVPR), IEEE Conference on*, pp. 604-611.2013.

[24] J. Wei, Y. Huang, K. Lu, and L. Wang, "Fields of Experts based multichannel compressed sensing," *Journal of Signal Processing Systems*, 2015.

[25] Y. Yu, J. Jin, F. Liu, and S. Crozier, "Multidimensional compressed sensing MRI using tensor decomposition-based sparsifying transform," *PLoS One*, vol. 9, no. 6, pp. e98441, 2014.

[26] S. Tan, Y. Zhang, G. Wang, X. Mou, G. Cao, Z. Wu, and H. Yu, "Tensor-based dictionary learning for dynamic tomographic reconstruction," *Phys Med Biol*, vol. 60, no. 7, pp. 2803-18, Apr 7, 2015.

[27] Y. Peng, D. Meng, Z. Xu, C. Gao, Y. Yang, and B. Zhang, "Decomposable nonlocal tensor dictionary learning for multispectral image denoising," in *(CVPR), IEEE Conference on*, pp. 2949-2956, 2014.

[28] W. Dong, G. Li, G. Shi, X. Li, and Y. Ma, "Low-rank tensor approximation with laplacian scale mixture modeling for multiframe image denoising," in *(ICCV), IEEE Conference on*, pp. 442-449, 2015.

[29] G. Chantas, N. P. Galatsanos, R. Molina, and A. K. Katsaggelos, "Variational bayesian image restoration with a product of spatially weighted total variationi mage priors," *IEEE Trans. Image Process*, vol. 19, pp. 351-362, 2010.

[30] S. Ravishankar and Y. Bresler, "MR image reconstruction from highly undersampled k-space data by dictionary learning," *IEEE Tran. Medical Imaging*, vol. 30, pp. 1028-1041, 2011.